

Nonreciprocal microwave–optical entanglement in Kerr-modified cavity optomagnomechanics

Ming-Yue Liu(刘明月), Yuan Gong(龚媛), Jiaojiao Chen(陈姣姣), Yan-Wei Wang(王艳伟), and Wei Xiong(熊伟)
Citation : Chin. Phys. B, 2025, 34 (**5**): 057202. DOI: 10.1088/1674-1056/adb735
http://cpb.iphy.ac.cn; http://iopscience.iop.org/cpb

What follows is a list of articles you may be interested in

Magnon-magnon coupling in noncollinear synthetic antiferromagnets

Tengfei Zhang(张腾飞), Quwen Wang(王曲文), Min Chen(陈敏), Jie Dong(董洁), Qian Zhao(赵乾), Zimu Li(李子木), Qingfang Liu(刘青芳), Jianbo Wang(王建波), and Jinwu Wei(魏晋武)
Chin. Phys. B, 2025, 34 (**5**): 057201. DOI: 10.1088/1674-1056/adb26b

Role of Ag microalloying on glass forming ability and crystallization kinetics of ZrCoAgAlNi amorphous alloy

A Surendar, K Geetha, C Rajan, and M Alaazim
Chin. Phys. B, 2021, 30 (**1**): 017201. DOI: 10.1088/1674-1056/abb65e

Spin Seebeck effect and spin Hall magnetoresistance in the $Pt/Y_3Fe_5O_{12}$ heterostructure under laser-heating

Shuanhu Wang(王拴虎), Gang Li(李刚), Jianyuan Wang(王建元), Yingyi Tian(田颖异), Hongrui Zhang(张洪瑞), Lvkuan Zou(邹吕宽), Jirong Sun(孙继荣), Kexin Jin(金克新)
Chin. Phys. B, 2018, 27 (**11**): 117201. DOI: 10.1088/1674-1056/27/11/117201

Direct spin-phonon coupling of spin-flip relaxation in quantum dots

Ji-Wen Yin(尹辑文), Wei-Ping Li(李伟萍), Hong-Juan Li(李红娟), Yi-Fu Yu(于毅夫)
Chin. Phys. B, 2017, 26 (**1**): 017201. DOI: 10.1088/1674-1056/26/1/017201

Interlayer transport of electron in bilayer graphene with phonon-induced lattice distortion in the presence of biased potential

He Liang-Ming (何良明)
Chin. Phys. B, 2013, 22 (**1**): 017201. DOI: 10.1088/1674-1056/22/1/017201

SPECIAL TOPIC — Advanced magnonics

Nonreciprocal microwave–optical entanglement in Kerr-modified cavity optomagnomechanics

Ming-Yue Liu(刘明月)[1], Yuan Gong(龚媛)[1], Jiaojiao Chen(陈姣姣)[1,2], Yan-Wei Wang(王艳伟)[1,†], and Wei Xiong(熊伟)[1,3,‡]

[1] *Department of Physics, Wenzhou University, Zhejiang* 325035, *China*
[2] *School of Physics and Optoelectronics Engineering, Anhui University, Hefei* 230601, *China*
[3] *International Quantum Academy, Shenzhen* 518048, *China*

(Received 27 December 2024; revised manuscript received 15 February 2025; accepted manuscript online 18 February 2025)

Microwave–optical entanglement is essential for efficient quantum communication, secure information transfer, and integrating microwave and optical quantum systems to advance hybrid quantum technologies. In this work, we demonstrate how the magnon Kerr effect can be harnessed to generate and control nonreciprocal entanglement in cavity optomagnomechanics (COMM). This effect induces magnon frequency shifts and introduces pair-magnon interactions, both of which are tunable through the magnetic field direction, enabling nonreciprocal behavior. By adjusting system parameters such as magnon frequency detuning, we show that magnon–phonon, microwave–optical photon–photon, and optical photon–magnon entanglement can be nonreciprocally enhanced and rendered more robust against thermal noise. Additionally, the nonreciprocity of entanglement can be selectively controlled, and ideal nonreciprocal entanglement is achievable. This work paves the way for designing nonreciprocal quantum devices across the microwave and optical regimes, leveraging the unique properties of the magnon Kerr effect in COMM.

Keywords: cavity optomechanics, cavity magnomechanics, continuous variable entanglement, magnon Kerr effect

PACS: 72.10.Di, 03.65.Ud, 43.25.Qp, 42.65.–k

DOI: 10.1088/1674-1056/adb735 **CSTR:** 32038.14.CPB.adb735

1. Introduction

Magnons,[1–4] the collective excitations of spins in magnetically ordered materials, are attracting increasing interest in quantum information science. Among these materials, yttrium-iron-garnet (YIG, $Y_3Fe_5O_{12}$)[5–7] is particularly notable for its high spin density and low loss.[8] In YIG, magnons can strongly couple with microwave photons in cavities,[8–11] enabling the exploration of phenomena such as dark modes,[12] non-Hermitian exceptional points,[13–18] one-way quantum steering,[19] dissipative coupling,[20,21] spin–photon interaction,[22] and near-perfect absorption.[23] Recently, cavity magnonics has entered the true quantum regime with the realization of single-magnon manipulation through coupling YIG and a superconducting qubit to a three-dimensional microwave cavity.[24,25]

Magnons can also couple with phonons via the magnetostrictive effect, forming the basis of cavity magnomechanics.[26] This coupling mirrors the radiation pressure mechanism in optomechanics,[27] allowing the direct transfer of optomechanical phenomena[27–32] into the magnomechanical domain. Magnomechanics further enables the study of tripartite entanglement,[33] squeezing,[34] and non-Hermitian physics.[35,36] Extending this framework, the mechanical motion in magnomechanics can couple to an optical cavity via radiation pressure, giving rise to cavity optomagnomechanics (COMM).[37,38] This hybrid platform provides a versatile foundation for exploring diverse quantum phenomena.[26]

In addition, the Kerr effect of magnons (i.e., Kerr magnons), stemming from the magnetocrystalline anisotropy in YIG,[39] was experimentally observed,[40,41] paving the way for investigating Kerr-modified quantum phenomena.[42,43] This nonlinearity facilitates the study of multistability,[43,44] spin–spin interactions,[45–47] and quantum phase transitions.[48,49] These findings emphasize the potential of magnons in hybrid quantum systems, where multiple quantum subsystems can be coupled for advanced quantum control and information processing. Additionally, Kerr magnons may be used to explore continuous variable entanglement,[50,51] although such entanglement has been largely confined to the microwave frequency domain. For broader quantum information applications, optical photons (or flying qubits) are preferred. Thus, achieving microwave–optical entanglement becomes critical. Various proposals have been put forward

†Corresponding author. E-mail: wangyw@wzu.edu.cn
‡Corresponding author. E-mail: xiongweiphys@wzu.edu.cn

© 2025 Chinese Physical Society and IOP Publishing Ltd. All rights, including for text and data mining, AI training, and similar technologies, are reserved.

in the context of hybrid electro-optomechanics,[52–58] where optical and microwave photons are coupled to a common mechanical motion via radiation pressure and capacitance change. Recently, microwave–optical entanglement has been extended to cavity magnomechanics through magnetostrictive forces.[59–61] The directionality dependence of the magnon Kerr effect in experiments[40,41] suggests that different magnetic field orientations can lead to opposite Kerr effects, which may introduce nonreciprocal behaviors in magnon-related hybrid systems.[50,51,62] Previous studies have demonstrated that nonreciprocity can enhance and protect continuous variable entanglement.[63] This raises the possibility that nonreciprocal magnon Kerr effects could enhance microwave–optical entanglement, although this has not yet been explored.

In this work, we propose a scheme for utilizing the magnon Kerr effect to generate and control nonreciprocal microwave–optical entanglement in COMM. The proposed system consists of a magnonic nanoresonator that is simultaneously coupled to both an optical cavity and a magnon mode via the radiation pressure and magnetostrictive force, respectively. The magnonic resonator is embedded within the microwave cavity, facilitating photon–magnon interactions. The optical cavity is constructed using a fixed mirror and a highly reflective, small, and lightweight mirror attached to the magnonic nanoresonator. Under strong driving fields, the magnon Kerr effect induces a frequency shift in the magnons, which can be either positive or negative, similar to the Sagnac effect.[64,65] This effect also gives rise to a pair-magnon interaction that regulates the values of all entanglement. Both the frequency shift and the coefficients of the pair-magnon interaction are sensitive to the direction of the external magnetic field, leading to nonreciprocal behavior in the entanglement. By tuning system parameters, such as magnon frequency detuning, we find that nonreciprocal enhancement of magnon–phonon, microwave–optical, and optical photon–magnon entanglements is possible when the magnetic field is changed. Furthermore, we demonstrate that ideal nonreciprocity of microwave–optical and optical photon–magnon entanglements is achievable through the defined bidirectional contrast ratio. This type of entanglement, transitioning from the microwave to the optical band, has broad applications in quantum information processing, particularly in quantum networks[66–69] and hybrid quantum systems.[70,71] Our work offers a promising avenue to employ the magnon Kerr effect for designing nonreciprocal quantum devices that operate across both microwave and optical bands in COMM. Note that our work differs from previous studies.[59–61] Compared to the works,[60,61] we employ an LC resonator rather than a 3D cavity. Additionally, magnons with the Kerr effect are introduced to investigate nonreciprocity, which distinguishes our approach from the study in Ref. [59], where the nonreciprocity arises from the Sagnac effect of photons.

This paper is organized as follows. In Section 2, the model and the system Hamiltonian are described. Then the dynamics of the system and the quantity of the bipartite entanglement are given in Section 3. In Section 4, the generation of nonreciprocal microwave–optical entanglement is studied. Finally, a conclusion is given in Section 5.

2. Model and hamiltonian

We consider a Kerr-modified COMM system comprising a microwave LC resonator (resonance frequency ω_a), a magnonic nanoresonator, and an optical cavity (resonance frequency ω_c), as illustrated in Fig. 1(a). The magnonic nanoresonator is modeled as a micro-scale bridge supporting both a magnon mode m (resonance frequency ω_m) with Kerr nonlinearity K_0 and a mechanical mode (resonance frequency ω_b). Through the magnetostrictive effect,[72] the magnon mode dispersively couples with the mechanical mode, forming a magnomechanical interaction. Additionally, the magnon mode is coupled to the microwave LC resonator, while the mechanical mode interacts dispersively with the optical cavity through radiation pressure.[27] The coupling mechanisms are schematically represented in Fig. 1(b). Note that the LC resonator can be modeled by either a coplanar-waveguide resonator or a transmission-line resonator. Experimentally, magnons in YIG materials have been strongly coupled to photons in the planar cavity structure.[9] Under the application of two driving fields, one to the optical cavity and the other to the magnon mode, the total Hamiltonian of the hybrid system can be expressed as (assuming $\hbar = 1$)

$$H = H_0 + H_{\rm om} + H_{\rm mm} + H_{\rm km} + H_{\rm drive}, \tag{1}$$

where

$$\begin{aligned} H_0 &= \omega_a a^\dagger a + \omega_c c^\dagger c + \omega_m m^\dagger m + \frac{\omega_b}{2}\left(q^2 + p^2\right), \\ H_{\rm om} &= -g_c c^\dagger c q, \quad H_{\rm mm} = g_m m^\dagger m q, \\ H_{\rm km} &= g_{am}(a^\dagger m + m^\dagger a) + K_0 (m^\dagger m)^2, \\ H_{\rm drive} &= {\rm i}\mathcal{E}_m m^\dagger {\rm e}^{-{\rm i}w_m t} + {\rm i}\mathcal{E}_c c^\dagger {\rm e}^{-{\rm i}w_c t} + {\rm H.c.} \end{aligned}$$

The first term, H_0, represents the free energy of the system. The second term, $H_{\rm om}$, denotes the optomechanical interaction between the mechanical mode and the optical cavity, characterized by the single-photon coupling strength g_c. The third term, $H_{\rm mm}$, describes the magnomechanical interaction between the mechanical mode and the magnon mode, with the single-magnon coupling strength g_m. The fourth term, $H_{\rm km}$, accounts for the coupling between the microwave LC resonator and the Kerr magnon mode, with a coupling strength g_{am}. Experimentally, g_{am} can reach the strong coupling regime, while the Kerr nonlinearity K_0 is tunable from negative to positive by varying the direction of the magnetic field.[41] The final term, $H_{\rm drive}$, represents the Hamiltonian of

the two driving fields, where $\mathcal{E}_c$ and $\mathcal{E}_m$ are the amplitudes and w_c and w_m are the frequencies. In Eq. (1), q and p denote the two quadratures of the mechanical resonator.

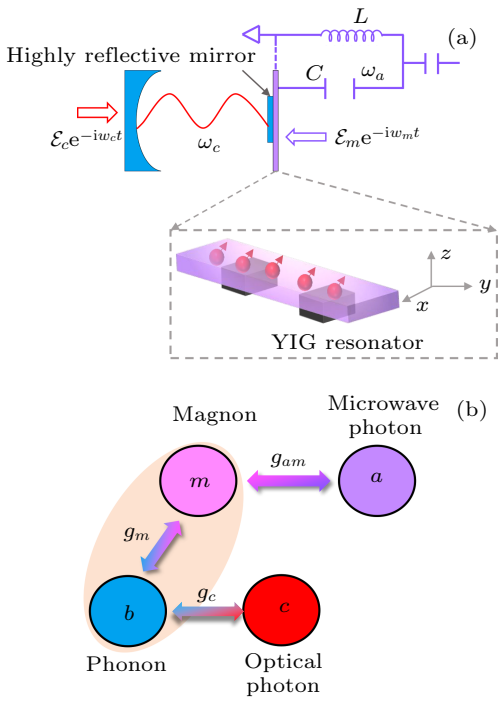


Fig. 1. (a) Schematic of the Kerr-modified COMM system consisting of an optical cavity, a YIG nanoresonator (see the bridge structure in the dashed box) and a microwave cavity (LC resonator), where the optical cavity is formed by two mirrors, one is fixed, the other is a highly reflective mirror attached to the YIG resonator. The YIG nanoresonator supports the Kerr magnons and phonon mode due to the magnetostrictive effect. The magnon Kerr effect stems from the magnetocrystallographic anisotropy, tuned by the magnetic field. $\mathcal{E}_{c(a)}$ is the driving field with frequency $w_{c(a)}$. (b) The coupling configuration. The mechanical mode is simultaneously coupled to both the optical photons and microwave magnons via the radiation pressure and magnetostrictive force, respectively. The coupling strengths are g_c and g_m. The magnons also interact with the microwave phonons with coupling strength g_{am}.

3. Dynamics and entanglement metric

When dissipation is included, the dynamics of the system can be governed by the quantum Langevin equations. In the rotating frame with respect to two driving fields, we have

$$\begin{aligned}
\dot{q} &= \omega_b p,\\
\dot{p} &= -\omega_b q-\gamma_b p+g_c c^{\dagger}c-g_m m^{\dagger}m+\xi,\\
\dot{a} &= -(\kappa_a+\mathrm{i}\Delta_a)a-\mathrm{i}g_{am}m+\sqrt{2\kappa_a}a_{\mathrm{in}},\\
\dot{c} &= -(\kappa_c+\mathrm{i}\Delta_c)c+\mathrm{i}g_c cq+\mathcal{E}_c+\sqrt{2\kappa_c}c_{\mathrm{in}},\\
\dot{m} &= -(\kappa_m+\mathrm{i}\Delta_m)m-\mathrm{i}g_m mq+\mathcal{E}_m+\sqrt{2\kappa_m}m_{\mathrm{in}}\\
&\quad -\mathrm{i}g_{am}a-2\mathrm{i}K_0 m^{\dagger}mm.
\end{aligned} \tag{2}$$

Here, $\Delta_{a(m)}=\omega_{a(m)}-w_m$ represents the detuning of the LC resonator (magnon mode) from the driving field with frequency w_m, while $\Delta_c=\omega_c-w_c$ is the detuning of the optical cavity from the driving field with frequency w_c. The decay rates of the LC resonator, optical cavity, magnon mode, and mechanical resonator are denoted by κ_a, κ_c, κ_m, and γ_b, respectively. σ_{in} ($\sigma=a,c,m$) are the input noise operators satisfying

$$\begin{aligned}
\langle\sigma_{\mathrm{in}}(t)\rangle &= 0,\\
\langle\sigma_{\mathrm{in}}^{\dagger}(t)\sigma_{\mathrm{in}}(t')\rangle &= n_\sigma(\omega_\sigma)\delta(t-t'),\\
\langle\sigma_{\mathrm{in}}(t)\sigma_{\mathrm{in}}^{\dagger}(t')\rangle &= [n_\sigma(\omega_\sigma)+1]\,\delta(t-t'),
\end{aligned} \tag{3}$$

where $n_\sigma(\omega_\sigma)=[\exp(\hbar\omega_\sigma/k_{\mathrm{B}}T)-1]^{-1}$ is the mean thermal excitation number at frequency ω_σ, k_{B} is the Boltzmann constant, and T is the bath temperature.

The mechanical resonator is also subject to a Brownian stochastic force $\xi(t)$, which is inherently non-Markovian. However, for a high mechanical quality factor $Q_b=\omega_b/\gamma_b\gg 1$, the force can be approximated as Markovian.[73,74] In this regime, $\xi(t)$ obeys

$$\langle\xi(t)\xi(t')+\xi(t')\xi(t)\rangle\simeq 2\gamma_b\,[2n_b(\omega_b)+1]\,\delta(t-t'), \tag{4}$$

where $n_b(\omega_b)$ is the mean thermal excitation number of the mechanical resonator, given by $n_b(\omega_b)=[\exp(\hbar\omega_b/k_{\mathrm{B}}T)-1]^{-1}$.

For long-time evolution, the system reaches its steady state, which implies that all time derivatives in Eq. (2) vanish. By assuming that $\langle\cdot\rangle$ denotes the steady-state value of the operator, we then have $\langle a\rangle=-g_{am}\langle m\rangle/\Delta_a$, $\langle c\rangle=-\mathrm{i}\mathcal{E}_c/\tilde{\Delta}_c$, $\langle p\rangle=0$, $\langle q\rangle=(g_c|\langle c\rangle|^2-g_m|\langle m\rangle|^2)/\omega_b$, and

$$\langle m\rangle=\frac{\mathrm{i}\mathcal{E}_m\Delta_a}{g_{am}^2-\left(\tilde{\Delta}_m+\Delta_k\right)\Delta_a}, \tag{5}$$

where $\tilde{\Delta}_m=\Delta_m+g_m\langle q\rangle$ and $\tilde{\Delta}_c=\Delta_c-g_c\langle q\rangle$ are effective detunings induced by the displacement of the mechanical resonator, $\Delta_k=2K_0|\langle m\rangle|^2$ represents the frequency shift induced by the magnon Kerr effect. In particular, Δ_k can be positive or negative, depending on the sign of K_0, which can be easily tuned by changing the magnetic field. To obtain the above results, we have assumed that the decay rate is much smaller than its corresponding effective frequency detuning.

With steady-state values in hand, we expand each operator around its steady-state value, i.e.,

$$\sigma=\langle\sigma\rangle+\delta\sigma,\quad q=\langle q\rangle+\delta q,\quad p=\langle p\rangle+\delta p, \tag{6}$$

where the symbol δ denotes the meaning of fluctuation. Substituting these expressions back into Eq. (2) and neglecting higher-order fluctuation terms ensured by the strong driving fields (e.g., $|\langle m\rangle|,|\langle c\rangle|\gg 1$),[28] the linearized dynamics for the fluctuations can be reduced to

$$\begin{aligned}
\delta\dot{q} &= \omega_b\delta p,\\
\delta\dot{p} &= -\omega_b\delta q-\gamma_b\delta p-\mathrm{i}G_c\left(\delta c^{\dagger}-\delta c\right)/\sqrt{2}\\
&\quad -\mathrm{i}G_m\left(\delta m^{\dagger}-\delta m\right)/\sqrt{2}+\xi,\\
\delta\dot{a} &= -(\kappa_a+\mathrm{i}\Delta_a)\,\delta a-\mathrm{i}g_{am}\delta m+\sqrt{2\kappa_a}a_{\mathrm{in}},\\
\delta\dot{m} &= -\left[\kappa_m+\mathrm{i}\left(\tilde{\Delta}_m+2\Delta_k\right)\right]\delta m-\mathrm{i}g_{am}\delta a\\
&\quad +G_m\delta q/\sqrt{2}+\mathrm{i}\Delta_k\delta m^{\dagger}+\sqrt{2\kappa_m}m_{\mathrm{in}},
\end{aligned}$$

$$\delta\dot{c} = -\left(\kappa_c + \mathrm{i}\tilde{\Delta}c\right)\delta c + G_c\delta q/\sqrt{2} + \sqrt{2\kappa_c}c_{\mathrm{in}}, \tag{7}$$

where $G_c = \mathrm{i}\sqrt{2}g_c\langle c\rangle$ is the enhanced optomechanical coupling by the multi-photon effect, and $G_m = -\mathrm{i}\sqrt{2}g_m\langle m\rangle$ is the enhanced magnomechanical coupling by multi-magnon effect.

By further introducing quadratures for the LC resonator, the optical cavity and the magnon mode, i.e., $\delta X_\sigma = \left(\sigma + \sigma^\dagger\right)/\sqrt{2}$ and $\delta Y_\sigma = \left(\sigma - \sigma^\dagger\right)/(\mathrm{i}\sqrt{2})$, the dynamics in Eq. (4) can be equivalently written as the matrix form

$$\dot{\boldsymbol{u}}(t) = \boldsymbol{A}\boldsymbol{u}(t) + \boldsymbol{n}(t), \tag{8}$$

where $\boldsymbol{u}(t) = [\delta X_a(t), \delta Y_a(t), \delta X_m(t), \delta Y_m(t), \delta q(t), \delta p(t), \delta X_c(t), \delta Y_c(t)]^{\mathrm{T}}$ is the vector operator of the system, $\boldsymbol{n}(t) = [\sqrt{2\kappa_a}X_a^{\mathrm{in}}(t), \sqrt{2\kappa_a}Y_a^{\mathrm{in}}(t), \sqrt{2\kappa_m}X_m^{\mathrm{in}}(t), \sqrt{2\kappa_m}Y_m^{\mathrm{in}}(t), 0, \xi(t), \sqrt{2\kappa_c}X_c^{\mathrm{in}}(t), \sqrt{2\kappa_c}Y_c^{\mathrm{in}}(t)]^{\mathrm{T}}$ is the vector operator of the input noise, and

$$\boldsymbol{A} = \begin{pmatrix} -\kappa_a & \Delta_a & 0 & g_{am} & 0 & 0 & 0 & 0 \\ -\Delta_a & -\kappa_a & -g_{am} & 0 & 0 & 0 & 0 & 0 \\ 0 & g_{am} & -\kappa_m & U & G_m & 0 & 0 & 0 \\ -g_{am} & 0 & -V & -\kappa_m & 0 & 0 & 0 & 0 \\ 0 & 0 & 0 & 0 & 0 & \omega_b & 0 & 0 \\ 0 & 0 & 0 & -G_m & -\omega_b & -\gamma_b & 0 & -G_c \\ 0 & 0 & 0 & 0 & G_c & 0 & -\kappa_c & \tilde{\Delta}_c \\ 0 & 0 & 0 & 0 & 0 & 0 & -\tilde{\Delta}_c & -\kappa_c \end{pmatrix} \tag{9}$$

is the drift matrix, where $U = \tilde{\Delta}_m + 3\Delta_k$ and $V = (\tilde{\Delta}_m + \Delta_k)$. According to the Routh–Hurwitz criterion,[75] when all eigenvalues of the matrix $\boldsymbol{A}$ have negative real parts, the system is stable. In what follows, the stability condition is ensured numerically.

When the system is stable, it reaches a unique steady state, independently of the initial condition. Since quantum noises $\xi(t)$ and $\sigma_{\mathrm{in}}(t)$ are zero-mean quantum Gaussian noises and the dynamics is linearized [see Eq. (4)], the quantum steady state for fluctuations is a zero-mean continuous variable Gaussian state, fully characterized by an 8×8 covariance matrix $\mathcal{V}_{lk}(\infty) = \frac{1}{2}\langle u_l(\infty)u_k(\infty) + u_k(\infty)u_l(\infty)\rangle$ $(l,k = 1,2,\ldots,8)$. The matrix $\mathcal{V}$ can be obtained by directly solving the Lyapunov equation[28]

$$\boldsymbol{A}\mathcal{V} + \mathcal{V}\boldsymbol{A}^{\mathrm{T}} + \mathcal{D} = 0, \tag{10}$$

where $\mathcal{D} = \mathrm{diag}[\kappa_a(2n_a+1), \kappa_a(2n_a+1), \kappa_m(2n_m+1), \kappa_m(2n_m+1), 0, \gamma_b(2n_b+1), \kappa_a(2n_c+1), \kappa_a(2n_c+1)]$ is defined by $\langle n_l(t)n_k(t') + n_k(t')n_l(t)\rangle = 2\mathcal{D}_{lk}\delta(t-t')$. Once the matrix $\mathcal{V}$ is obtained by solving Eq. (7), arbitrary bipartite entanglement can be quantified by the logarithmic negativity[76–78]

$$E_{\mathrm{N}} \equiv \max[0, -\ln 2\eta^-] \tag{11}$$

with

$$\eta^- = 2^{-1/2}[\Sigma - (\Sigma^2 - 4\det\mathcal{V}_4)^{1/2}]^{1/2}, \tag{12}$$

where $\Sigma = \det\mathcal{A} + \det\mathcal{B} - 2\det\mathcal{C}$ and $\mathcal{V}_4 = \begin{pmatrix} \mathcal{A} & \mathcal{C} \\ \mathcal{C}^{\mathrm{T}} & \mathcal{B} \end{pmatrix}$ is the 4×4 block form of the correlation matrix, associated with two modes of interest.[79] $\mathcal{A}$, $\mathcal{B}$, and $\mathcal{C}$ are the 2×2 blocks of $\mathcal{V}_4$. A positive logarithmic negativity ($E_{\mathrm{N}} > 0$) denotes the presence of bipartite entanglement of the two modes of interest in the considered system.

4. Nonreciprocal microwave–optical entanglement

In our setup, there are two kinds of microwave–optical entanglement, i.e., entanglement between photons in the optical cavity and photons in the microwave LC resonator (E_{N}^{ac}) or magnons in the magnon mode (E_{N}^{mc}).

4.1. Nonreciprocal magnon–phonon entanglement

To study them, we operate the optical cavity at the red sideband ($\tilde{\Delta}_c = \omega_b$) and the magnon mode at the blue sideband ($\tilde{\Delta}_m = -\omega_b$). This is because, at the magnon blue sideband, the Stokes scattering process is dominant, giving rise to entanglement between magnons and phonons. But to observe it, cooling the mechanical resonator to the ground state is crucial, thus we need to operate the optical cavity at the red sideband to activate the anti-Stokes scattering process, then the mechanical resonator can be significantly cooled to its ground state by transferring the thermal phonons to the optical cavity. These two effects allow the optimal magnon–phonon entanglement observed, as demonstrated by Fig. 2(a), in which the following feasible parameters are chosen:[43,80] $\omega_a/2\pi = 10$ GHz, $\omega_b/2\pi = 40$ MHz, $\omega_c/2\pi = 190$ THz, $\kappa_a/2\pi = \kappa_m/2\pi = 1$ MHz, $\kappa_c/2\pi = 2$ MHz, $\gamma_b/2\pi = 100$ Hz, $g_{am}/2\pi = 4$ MHz, $G_m/2\pi = 2$ MHz, $G_c/2\pi = 8$ MHz, $T = 10$ mK.

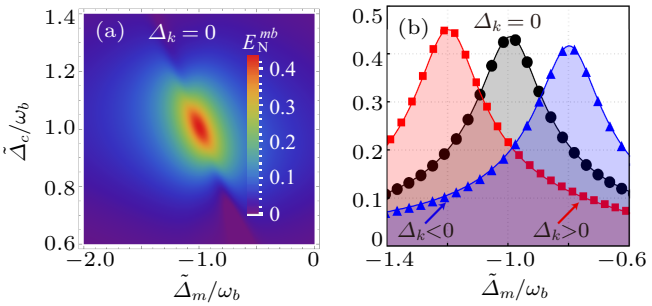


Fig. 2. (a) Density plot of the magnon–phonon entanglement E_{N}^{mb} vs. the normalized parameters $\tilde{\Delta}_m/\omega_b$ and $\tilde{\Delta}_c/\omega_b$ without the magnon Kerr effect $\Delta_k = 0$, where $\Delta_a = -\omega_b$. (b) The magnon–phonon entanglement E_{N}^{mb} vs. the normalized parameter $\tilde{\Delta}_m/\omega_b$ with and without the magnon Kerr effect, where $\omega_a/2\pi = 10$ GHz, $\omega_b/2\pi = 40$ MHz, $\omega_c/2\pi = 190$ THz, $\Delta_a = -\omega_b$, $\tilde{\Delta}_c = \omega_b$, $\kappa_a/2\pi = \kappa_m/2\pi = 1$ MHz, $\kappa_c/2\pi = 2$ MHz, $\gamma_b/2\pi = 100$ Hz, $g_{am}/2\pi = 4$ MHz, $G_m/2\pi = 2$ MHz, $G_c/2\pi = 8$ MHz, $T = 10$ mK, $|\Delta_k| = 0.1\omega_b$.

In Fig. 2(a), the magnon Kerr effect is not taken into account (i.e., $\Delta_k = 0$). In fact, the magnon Kerr effect can give rise to nonreciprocal magnon–phonon entanglement, as illustrated by Fig. 2(b), where the optical cavity is fixed at the red

sideband ($\tilde{\Delta}_c = \omega_b$). Specifically, when the Kerr coefficient is positive ($K_0 > 0$), the caused shift $\Delta_k > 0$, leading to a left-shift for the magnon–phonon entanglement (see the red line). But when $K_0 < 0$, we have $\Delta_k < 0$, in this case we find the magnon–phonon entanglement has a right-shift (see the blue line). In addition, the value of the maximal magnon–phonon entanglement also exhibits different behaviors when Δ_k is tuned from the positive ($\Delta_k > 0$) to negative ($\Delta_k < 0$). These differences come from the pair-magnon effect induced by linearization of the magnon Kerr effect. When $\Delta_k = 0.1\omega_b > 0$, the maximal value of the magnon–phonon entanglement is located at $\tilde{\Delta}_m \approx -1.2\omega_b$. But when $\Delta_k = -0.1\omega_b < 0$, it is located at $\tilde{\Delta}_m \approx -0.8\omega_b$. The precise evaluation is given by $\tilde{\Delta}_m \approx -\omega_b - 2\Delta_k$. This is because in the presence of the magnon Kerr effect, the effective frequency detuning indeed becomes $\tilde{\Delta}_m + 2\Delta_k$ [see the term related to δm in Eq. (7)].

To explain why entanglement is enhanced (reduced) when $\Delta_k > 0$ (< 0), one can check that the mean magnon number increases (decreases) when $\Delta_k > 0$ (< 0), which is directly obtained from Eq. (5). Specifically, given that $\Delta_a = -\omega_b$ and $\tilde{\Delta}_m < 0$ are chosen [see Fig. 2(b)], $\Delta_k\tilde{\Delta}_m > 0$ (i.e., $\Delta_k < 0$) results in a decrease in the mean magnon number. Conversely, when $\Delta_k\tilde{\Delta}_m < 0$ (i.e., $\Delta_k > 0$), the mean magnon number increases. A larger mean magnon number corresponds to a stronger effective magnomechanical coupling strength [see Eq. (7)], giving rise to strong entanglement. Therefore, the sign of Δ_k directly influences the statistics of the mean magnon number, thereby indirectly enhancing or weakening the effective magnomechanical coupling strength for quantum entanglement generation.

4.2. Nonreciprocal microwave–optical photon–photon entanglement

Due to beam splitter interactions including the optical photon–phonon coupling and the microwave photon–magnon coupling, the established magnon–phonon entanglement in Fig. 2(a) is distributed to both the subsystems of optomechanics and cavity magnonics, leading to indirect microwave–optical photon–photon entanglement. When the red-sideband optical photons are resonant with the phonons, while the microwave photons are resonant with the magnons, the microwave–optical photon–photon entanglement can be optimal, as clearly demonstrated by Figs. 3(a) and 3(b). Figure 3(c) further illustrates the nonreciprocal behavior of the microwave–optical photon–photon entanglement versus the normalized magnon detuning $\tilde{\Delta}_m/\omega_b$ induced by the magnon Kerr effect, where $\Delta_a = -\omega_b$ and $\tilde{\Delta}_c = \omega_b$ are fixed. One can obviously see that the microwave–optical photon–photon entanglement has a similar behavior to the magnon–phonon entanglement in Fig. 2(b) when the magnon Kerr coefficient is tuned from negative to positive. We also examine the behavior of the microwave–optical photon–photon entanglement with the normalized parameters $\tilde{\Delta}_m/\omega_b$ and Δ_k/ω_b in Fig. 3(d). We find that the optimal microwave–optical photon–photon entanglement is realized only when $\tilde{\Delta}_m \simeq -0.4\Delta_k^2/\omega_b - 2.06\Delta_k - \omega_b$ is satisfied (see the white dashed line). When this condition is satisfied, we show that the optimal microwave–optical photon–photon entanglement can be enhanced in the region of $\Delta_k > 0$ compared to the case without the magnon Kerr effect ($\Delta_k = 0$). However, in the region of $\Delta_k < 0$, the optimal microwave–optical photon–photon entanglement is significantly weakened. Moreover, the optimal microwave–optical photon–photon entanglement decreases monotonically with Δ_k in the region of $\Delta_k < 0$, while it increases first and then decreases with Δ_k in the region of $\Delta_k > 0$, as illustrated in Fig. 3(e). In fact, the microwave–optical photon–photon entanglement can also be tuned by varying the linearized optomechanical coupling G_c, as demonstrated by Fig. 3(f). By introducing the magnon Kerr effect, we show that the optimal microwave–optical photon–photon entanglement can be nonreciprocally enhanced. At the same time, we find that the microwave–optical photon–photon entanglement can be nonreciprocally robust against the bath temperature [see Fig. 3(g)]. More importantly, the introduced magnon Kerr effect can significantly improve the survival temperature of the microwave–optical photon–photon entanglement.

4.3. Nonreciprocal optical photon–magnon entanglement

When the magnon–phonon entanglement is generated, the phonon mediated optical photon–magnon entanglement can also be produced because the beam splitter interaction between the optical photons and phonons allows the entanglement to be redistributed to the subsystem of the optomechanics. To produce nonreciprocal optical photon–magnon entanglement, the magnon Kerr effect is introduced. Comparing Fig. 4(a) with Fig. 3(b), the complementary entanglement distribution clearly shows that breaking the microwave photon–magnon resonance ($\Delta_a \neq \tilde{\Delta}_m$) is beneficial to generate the optical photon–magnon entanglement. Figure 4(b) shows that the optical photon–magnon entanglement has opposite behaviors when the sign of the Kerr coefficient is opposite. To obtain the optimal entanglement in the presence of the magnon Kerr effect, the condition $\tilde{\Delta}_m \simeq -0.45\Delta_k^2/\omega_b - 2.1\Delta_k - 0.91\omega_b$ must be approximately satisfied, which is given by the white dashed curve in Fig. 4(c). When this optimal condition is kept, the optimal optical photon–magnon entanglement has the similar behavior with the optimal microwave–optical photon–photon entanglement in Fig. 3(e) by tuning the Kerr coefficient from negative (positive) to positive (negative), as demonstrated by Fig. 4(d). Obviously, the optimal optical photon–magnon entanglement decreases with increasing Δ_k in the region of $\Delta_k < 0$. However, in the region of $\Delta_k > 0$, the optimal op-

tical photon–magnon entanglement increases first and then decreases with increasing Δ_k. This indicates that the optical photon–magnon entanglement can be nonreciprocally enhanced by the magnon Kerr effect. Figure 4(e) further shows that the optical photon–magnon entanglement can be tuned by the linearized optomechanical coupling strength. Besides, by introducing the magnon Kerr effect, not only the optical photon–magnon entanglement has nonreciprocal behaviors, but also a stronger optomechanical coupling is required to obtain the optimal optical photon–magnon entanglement. Figure 4(f) indicates that nonreciprocity induced by the magnon Kerr effect not only can lead to the optical photon–magnon entanglement being more robust against the bath temperature, but also can improve the entanglement survival temperature.

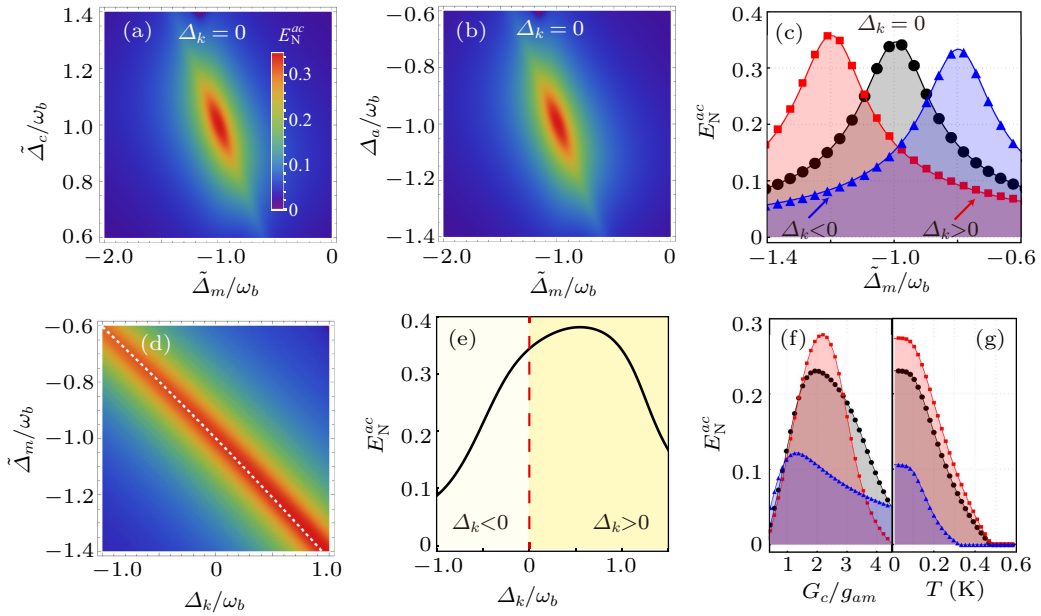


Fig. 3. Density plot of the microwave–optical photon–photon entanglement E_N^{ac} vs. the normalized parameters (a) $\tilde{\Delta}_m/\omega_b$ and $\tilde{\Delta}_c/\omega_b$, (b) $\tilde{\Delta}_m/\omega_b$ and Δ_a/ω_b without the magnon Kerr effect. (c) The microwave–optical photon–photon entanglement E_N^{ac} vs. the normalized parameter $\tilde{\Delta}_m/\omega_b$ with and without the magnon Kerr effect. (d) Density plot of the microwave–optical photon–photon entanglement E_N^{ac} vs. the normalized parameters $\tilde{\Delta}_m/\omega_b$ and Δ_k/ω_b. The microwave–optical photon–photon entanglement E_N^{ac} vs. (e) Δ_k/ω_b, with $\tilde{\Delta}_m = -0.4\Delta_k^2/\omega_b - 2.06\Delta_k - \omega_b$, (f) G_c/g_{am} with $\tilde{\Delta}_m/\omega_b = -1.11$, and (g) the bath temperature T with $\tilde{\Delta}_m/\omega_b = -1.11$. In (a)–(g), $|\Delta_k| = 0.1\omega_b$ and $\Delta_a = -\tilde{\Delta}_c = -\omega_b$ are taken. Other parameters are the same as those in Fig. 2.

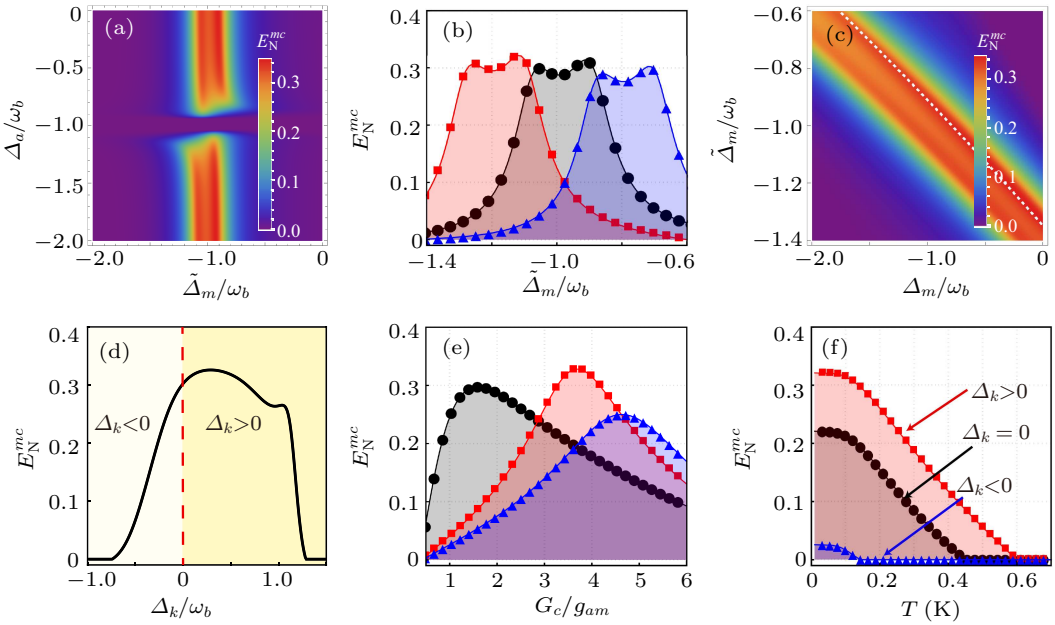


Fig. 4. Density plot of the optical photon–magnon entanglement E_N^{mc} vs. the normalized parameters (a) $\tilde{\Delta}_m/\omega_b$ and $\tilde{\Delta}_c/\omega_b$, without the magnon Kerr effect. (b) The optical photon–magnon entanglement E_N^{mc} vs. the normalized parameter $\tilde{\Delta}_m/\omega_b$ with and without the magnon Kerr effect. (c) Density plot of the optical photon–magnon entanglement E_N^{mc} vs. the normalized parameters $\tilde{\Delta}_m/\omega_b$ and Δ_k/ω_b. (d) The optical photon–magnon entanglement E_N^{mc} vs. Δ_k/ω_b, with $\tilde{\Delta}_m = -0.45\Delta_k^2/\omega_b - 2.1\Delta_k - 0.91\omega_b$. The optical photon–magnon entanglement E_N^{mc} vs. (e) the normalized parameter G_c/g_{am} with $\tilde{\Delta}_m/\omega_b = -1$, and (f) the bath temperature T with $\tilde{\Delta}_m/\omega_b = -1.11$. In (a)–(f), $|\Delta_k| = 0.1\omega_b$, $\Delta_a = 0, \tilde{\Delta}_c = \omega_b$. Other parameters are the same as those in Fig. 2.

4.4. Bidirectional contrast ratio

To quantitatively describe nonreciprocal entanglement induced by the magnon Kerr effect, we introduce the bidirectional contrast ratio χ (satisfying $0 \leq \chi \leq 1$) for bipartite entanglement to show nonreciprocity, i.e.,

$$\chi_E^{ij} = \frac{\left|E_{\rm N}^{ij}(>0) - E_{\rm N}^{ij}(<0)\right|}{E_{\rm N}^{ij}(>0) + E_{\rm N}^{ij}(<0)}. \tag{13}$$

The parameter χ_E^{ij} equals 1 for ideal nonreciprocity and 0 for no nonreciprocity in bipartite entanglement. A higher contrast ratio χ indicates stronger nonreciprocity. To clarify this, we numerically plot the bidirectional contrast ratio χ as a function of frequency detuning $\tilde{\Delta}_m$ in Fig. 5(a). The figure demonstrates that by tuning $\tilde{\Delta}_m$, the nonreciprocity of the microwave–optical photon–photon entanglement and the optical photon–magnon entanglement can be switched on or off. Moreover, the bidirectional contrast ratio for both types of entanglement can be adjusted from 0 to 1 by varying $\tilde{\Delta}_m$, indicating that ideal nonreciprocity for the microwave–optical photon–photon entanglement and the optical photon–magnon entanglement can be achieved by controlling the magnon frequency detuning.

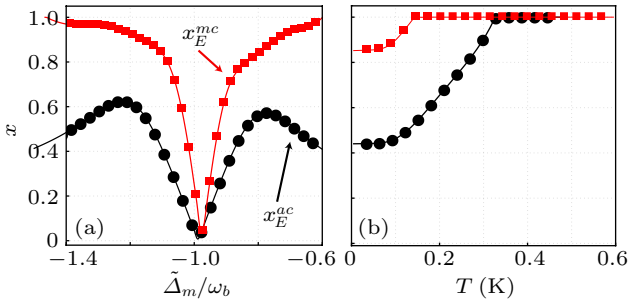


Fig. 5. Bidirectional contrast ratio χ vs. the normalized parameters (a) $\tilde{\Delta}_m/\omega_b$ and (b) the bath temperature T, where $|\Delta_k| = 0.1\omega_b$. Other parameters are the same as those in Fig. 2.

The effect of the bath temperature on the bidirectional contrast is further examined in Fig. 5(b). The results show that the nonreciprocity of the microwave–optical photon–photon entanglement and the optical photon–magnon entanglement gradually increases with increasing the bath temperature. Interestingly, ideal nonreciprocity for both entanglements can be realized at higher temperatures, indicating that elevated temperatures are beneficial for achieving optimal nonreciprocal entanglement.

5. Conclusion

In summary, we propose a novel scheme that leverages the magnon Kerr effect to generate and control nonreciprocal microwave–optical entanglement in cavity COMM. By utilizing the strong coupling between a magnonic resonator, a microwave cavity, and an optical cavity, we demonstrate how the direction of the external magnetic field can be exploited to induce nonreciprocal behavior in entanglement dynamics. We show that tuning parameters, such as the magnon frequency detuning, allows for enhanced nonreciprocal entanglement across multiple domains, including magnon–phonon, microwave–optical, and photon–magnon entanglements. Moreover, our findings highlight the potential for achieving ideal nonreciprocity in microwave–optical and photon–magnon entanglements, which is crucial for quantum information processing and quantum networks. This work provides a promising path for designing nonreciprocal quantum devices capable of operating across both microwave and optical bands, contributing to the development of hybrid quantum systems and advanced quantum technologies.

Acknowledgements

WX is supported by the Natural Science Foundation of Zhejiang Province (Grant No. LY24A040004), the "Pioneer" and "Leading Goose" R&D Program of Zhejiang (Grant No. 2025C01028), and the Shenzhen International Quantum Academy (Grant No. SIQA2024KFKT010). YWW is supported by the Natural Science Foundation of Zhejiang Province (Grant No. LY23A40002) and Wenzhou Science and Technology Plan Project (Grant No. L20240004).

References

[1] Rameshti B Z, Kusminskiy S V, Haigh J A, Usami K, Lachance-Quirion D, Nakamura Y, Hu C M, Tang H X, Bauer G E and Blanter Y M 2022 *Phys. Rep.* **979** 1
[2] Yuan H, Cao Y, Kamra A, Duine R A and Yan P 2022 *Phys. Rep.* **965** 1
[3] Prabhakar A and Stancil D D 2009 *Spin Waves: Theory and applications* (Springer)
[4] Van Kranendonk J and Van Vleck J 1958 *Rev. Mod. Phys.* **30** 1
[5] Schmidt G, Hauser C, Trempler P, Paleschke M and Papaioannou E T 2020 *Phys. Status Solidi (b)* **257** 1900644
[6] Mallmann E, Sombra A, Goes J and Fechine P 2013 *Solid State Phenom.* **202** 65
[7] Geller S and Gilleo M 1957 *J. Phys. Chem. Solids* **3** 30
[8] Li Y, Zhang W, Tyberkevych V, Kwok W K, Hoffmann A and Novosad V 2020 *J. Appl. Phys.* **128** 130902
[9] Huebl H, Zollitsch C W, Lotze J, Hocke F, Greifenstein M, Marx A, Gross R and Goennenwein S T 2013 *Phys. Rev. Lett.* **111** 127003
[10] Tabuchi Y, Ishino S, Ishikawa T, Yamazaki R, Usami K and Nakamura Y 2014 *Phys. Rev. Lett.* **113** 083603
[11] Zhang X, Zou C L, Jiang L and Tang H X 2014 *Phys. Rev. Lett.* **113** 156401
[12] Zhang X, Zou C L, Zhu N, Marquardt F, Jiang L and Tang H X 2015 *Nat. Commun.* **6** 8914
[13] Zhang D, Luo X Q, Wang Y P, Li T F and You J 2017 *Nat. Commun.* **8** 1368
[14] Zhang X, Ding K, Zhou X, Xu J and Jin D 2019 *Phys. Rev. Lett.* **123** 237202
[15] Zhao J, Liu Y, Wu L, Duan C K, Liu Y X and Du J 2020 *Phys. Rev. Appl.* **13** 014053
[16] Sadovnikov A V, Zyablovsky A A, Dorofeenko A V and Nikitov S A 2022 *Phys. Rev. Appl.* **18** 024073
[17] Liu H, Sun D, Zhang C, Groesbeck M, Mclaughlin R and Vardeny Z V 2019 *Sci. Adv.* **5** eaax9144
[18] Cao Y and Yan P 2019 *Phys. Rev. B* **99** 214415
[19] Yang Z B, Liu X D, Yin X Y, Ming Y, Liu H Y and Yang R C 2021 *Phys. Rev. Appl.* **15** 024042

[20] Wang Y P, Rao J, Yang Y, Xu P C, Gui Y, Yao B, You J and Hu C M 2019 *Phys. Rev. Lett.* **123** 127202
[21] Harder M, Yao B, Gui Y and Hu C M 2021 *J. Appl. Phys.* **129** 201101
[22] Hei X L, Dong X L, Chen J Q, Shen C P, Qiao Y F and Li P B 2021 *Phys. Rev. A* **103** 043706
[23] Rao J, Xu P, Gui Y, Wang Y, Yang Y, Yao B, Dietrich J, Bridges G, Fan X, Xue D, *et al*. 2021 *Nat. Commun.* **12** 1933
[24] Xu D, Gu X K, Li H K, Weng Y C, Wang Y P, Li J, Wang H, Zhu S Y and You J 2023 *Phys. Rev. Lett.* **130** 193603
[25] Xu D, Gu X K, Weng Y C, Li H K, Wang Y P, Zhu S Y and You J 2024 *Quantum Science and Technology* **9** 035002
[26] Zuo X, Fan Z Y, Qian H, Ding M S, Tan H, Xiong H and Li J 2024 *New J. Phys.* **26** 031201
[27] Aspelmeyer M, Kippenberg T J and Marquardt F 2014 *Rev. Mod. Phys.* **86** 1391
[28] Vitali D, Gigan S, Ferreira A, Böhm H, Tombesi P, Guerreiro A, Vedral V, Zeilinger F A and Aspelmeyer M 2007 *Phys. Rev. Lett.* **98** 030405
[29] Xiong W, Li Z, Zhang G Q, Wang M, Li H C, Luo X Q and Chen J 2022 *Phys. Rev. A* **106** 033518
[30] Xiong W, Li Z, Song Y, Chen J, Zhang G Q and Wang M 2021 *Phys. Rev. A* **104** 063508
[31] Xiong W, Jin D Y, Qiu Y, Lam C H and You J 2016 *Phys. Rev. A* **93** 023844
[32] Kani A, Sarma B and Twamley J 2022 *Phys. Rev. Lett.* **128** 013602
[33] Li J, Zhu S Y and Agarwal G 2018 *Phys. Rev. Lett.* **121** 203601
[34] Li J, Zhu S Y and Agarwal G 2019 *Phys. Rev. A* **99** 021801
[35] Lu T X, Zhang H, Zhang Q and Jing H 2021 *Phys. Rev. A* **103** 063708
[36] He W D, Fan X H, Liu M Y, Zhang G Q, Li H C and Xiong W 2025 *Adv. Quantum Tech.* **8** 2400275
[37] Fan Z Y, Qiu L, Gröblacher S and Li J 2023 *Laser & Photonics Reviews* **17** 2200866
[38] Fan Z Y, Shen R C, Wang Y P, Li J and You J 2022 *Phys. Rev. A* **105** 033507
[39] Zhang G, Wang Y and You J 2019 *Science China Physics, Mechanics & Astronomy* **62** 14601
[40] Wang Y P, Zhang G Q, Zhang D, Luo X Q, Xiong W, Wang S P, Li T F, Hu C M and You J 2016 *Phys. Rev. B* **94** 224410
[41] Wang Y P, Zhang G Q, Zhang D, Li T F, Hu C M and You J 2018 *Phys. Rev. Lett.* **120** 057202
[42] Zheng S, Wang Z, Wang Y, Sun F, He Q, Yan P and Yuan H 2023 *J. Appl. Phys.* **134** 151101
[43] Shen R C, Li J, Fan Z Y, Wang Y P and You J 2022 *Phys. Rev. Lett.* **129** 123601
[44] Bi M, Yan X, Zhang Y and Xiao Y 2021 *Phys. Rev. B* **103** 104411
[45] Xiong W, Tian M, Zhang G Q and You J 2022 *Phys. Rev. B* **105** 245310
[46] Xiong W, Wang M, Zhang G Q and Chen J 2023 *Phys. Rev. A* **107** 033516
[47] He W D, Fan X H, Liu M Y, Wang M F, Zhang G Q, Li H C and Xiong W 2025 *Opt. Lett.* **50** 1516
[48] Zhang G Q, Chen Z, Xiong W, Lam C H and You J 2021 *Phys. Rev. B* **104** 064423
[49] Liu G, Xiong W and Ying Z J 2023 *Phys. Rev. A* **108** 033704
[50] Chen J, Fan X G, Xiong W, Wang D and Ye L 2024 *Phys. Rev. A* **109** 043512
[51] Chen J, Fan X G, Xiong W, Wang D and Ye L 2023 *Phys. Rev. B* **108** 024105
[52] Zhong C, Han X, Tang H X and Jiang L 2020 *Phys. Rev. A* **101** 032345
[53] Barzanjeh S, Abdi M, Milburn G J, Tombesi P and Vitali D 2012 *Phys. Rev. Lett.* **109** 130503
[54] Wu J, Cui C, Fan L and Zhuang Q 2021 *Phys. Rev. Appl.* **16** 064044
[55] Zhong C, Wang Z, Zou C, Zhang M, Han X, Fu W, Xu M, Shankar S, Devoret M H, Tang H X, *et al*. 2020 *Phys. Rev. Lett.* **124** 010511
[56] Meesala S, Lake D, Wood S, Chiappina P, Zhong C, Beyer A D, Shaw M D, Jiang L and Painter O 2024 *Phys. Rev. X* **14** 031055
[57] Wei T, Wu D, Miao Q, Yang C and Luo J 2022 *Opt. Express* **30** 10135
[58] Sahu R, Qiu L, Hease W, Arnold G, Minoguchi Y, Rabl P and Fink J M 2023 *Science* **380** 718
[59] Zheng Q, Zhong W, Cheng G and Chen A 2024 *J. Appl. Phys.* **135** 084401
[60] Zuo X, Fan Z Y, Qian H, Ding M S, Tan H, Xiong H and Li J 2024 *New J. Phys.* **26** 031201
[61] Li H T, Fan Z Y, Zhu H B, Gröblacher S and Li J 2025 *Laser & Photonics Reviews* 2401348
[62] Fan X H, Zhang Y N, Yu J P, Liu M Y, He W D, Li H C and Xiong W 2024 *Adv. Quantum Tech.* **7** 2400043
[63] Jiao Y F, Zhang S D, Zhang Y L, Miranowicz A, Kuang L M and Jing H 2020 *Phys. Rev. Lett.* **125** 143605
[64] Maayani S, Dahan R, Kligerman Y, Moses E, Hassan A U, Jing H, Nori F, Christodoulides D N and Carmon T 2018 *Nature* **558** 569
[65] Malykin G B 2000 *Physics-Uspekhi* **43** 1229
[66] Schoelkopf R and Girvin S 2008 *Nature* **451** 664
[67] Pirandola S and Braunstein S L 2016 *Nature* **532** 169
[68] Krastanov S, Raniwala H, Holzgrafe J, Jacobs K, Lončar M, Reagor M J and Englund D R 2021 *Phys. Rev. Lett.* **127** 040503
[69] Agustí J, Minoguchi Y, Fink J M and Rabl P 2022 *Phys. Rev. A* **105** 062454
[70] Xiang Z L, Ashhab S, You J and Nori F 2013 *Rev. Mod. Phys.* **85** 623
[71] Clerk A, Lehnert K, Bertet P, Petta J and Nakamura Y 2020 *Nat. Phys.* **16** 257
[72] Zhang X, Zou C L, Jiang L and Tang H X 2016 *Sci. Adv.* **2** e1501286
[73] Benguria R and Kac M 1981 *Phys. Rev. Lett.* **46** 1
[74] Giovannetti V and Vitali D 2001 *Phys. Rev. A* **63** 023812
[75] DeJesus E X and Kaufman C 1987 *Phys. Rev. A* **35** 5288
[76] Vidal G and Werner R F 2002 *Phys. Rev. A* **65** 032314
[77] Adesso G, Serafini A and Illuminati F 2004 *Phys. Rev. A* **70** 022318
[78] Plenio M B 2005 *Phys. Rev. Lett.* **95** 090503
[79] Simon R 2000 *Phys. Rev. Lett.* **84** 2726
[80] Potts C A, Varga E, Bittencourt V A, Kusminskiy S V and Davis J P 2021 *Phys. Rev. X* **11** 031053